Synthesis, Biological Evaluation, and Molecular Modeling Studies of a Novel, Peripherally Selective Inhibitor of Catechol-*O*-methyltransferase

David A. Learmonth,[†] P. Nuno Palma,[‡] Maria A. Vieira-Coelho,[‡,§] and Patrício Soares-da-Silva*[,‡]

Laboratory of Chemistry and Laboratory of Pharmacology, Department of Research & Development, BIAL, 4745-457 S. Mamede do Coronado, Portugal

Received May 25, 2004

A novel series of potent, peripherally selective, and long-acting inhibitors of catechol-*O*-methyltransferase (COMT) has been synthesized. The introduction and nature of heteroatom-containing substituents to the side-chain of the nitrocatechol pharmacophore was found to have a profound effect on both peripheral selectivity and duration of COMT inhibition in the mouse. This approach led to the discovery of 1-(3,4-dihydroxy-5-nitrophenyl)-3-[4-[3-(trifluoromethyl)-phenyl]-1-piperazinyl]-1-propanone hydrochloride **35** (BIA 3−335), which was found to possess a superior inhibitory profile in vivo over both the nonselective inhibitor tolcapone **1** and the peripherally selective but short-acting entacapone **2**. In this model, **35** retained 75% inhibition of peripheral COMT at 6 h after oral administration, yet significantly, only a minor reduction of central (cerebral) COMT activity was observed. Molecular modeling techniques were applied to review the analysis of the ternary enzyme−inhibitor complex previously determined by X-ray crystallography and to provide a deeper understanding of the structure−activity relationships within this novel series. Furthermore, a computational approach was applied in an effort to elucidate the particular structural factors relevant to the poor blood−brain permeability of **35**. In conclusion, the improved biological properties herein reported reveal **35** as a candidate for clinical studies as an adjunct to L-DOPA therapy for Parkinson's disease.

Introduction

Catechol-*O*-methyltransferase (COMT)[1] is a magnesium-dependent enzyme found in both the periphery and central nervous system (CNS) that catalyses the transfer of a methyl group from its cofactor *S*-adenosyl-L-methionine (SAM) to one hydroxyl group of a substrate bearing the catechol motif via an S_N2-type reaction, giving rise to an *O*-methylated catechol and *S*-adenosylhomocysteine. COMT is known to play an important role in the inactivation of endogenous neuroactive catecholamines[2] such as dopamine and in the detoxification of several xenobiotic catechols.[3,4] In recent years, our group and others have been greatly interested in the development of tight-binding, reversible inhibitors of COMT as adjuncts[5] to L-3,4-dihydroxyphenylalanine (L-DOPA) therapy for Parkinson's disease[6] (PD, a neurodegenerative disorder characterized by a deficiency of cerebral dopamine). This attraction has been based on the premise that COMT inhibition could significantly reduce the extent of *O*-methylation of L-DOPA to 3-*O*-methyl-L-DOPA (3-OMD), which is the principal metabolic pathway for L-DOPA in peripheral tissues when L-DOPA is coadministered with a peripheral decarboxylase inhibitor such as carbidopa.[7] Inhibition of COMT could thereby increase L-DOPA bioavailability, providing an improvement in the percentage of the administered L-DOPA dose penetrating into the brain. Further still, it has been observed that the *O*-methylated metabolite 3-OMD has a comparatively long in vivo elimination half-life and tends to accumulate in tissues.[8] Since this metabolite actually competes with L-DOPA for transport across the blood−brain barrier (BBB), it would be anticipated that a reduction in circulating 3-OMD levels should permit improved passage of L-DOPA across the BBB into the brain.

So-called "second-generation" COMT inhibitors[9,10] incorporate the nitrocatechol subunit and are typified by tolcapone **1**[11] and entacapone **2**[12] (Figure 1). Although both structures share the same pharmacophore, the pharmacological profile of **1** differs from that of **2** in that it is characterized as an indiscriminate inhibitor of both central and peripheral COMT, whereas **2** is essentially a peripheral inhibitor. The issue of selectivity in COMT inhibition has been the subject of some debate, although we, and others, have hypothesized that central inhibition may be of less consequence should the principal role of COMT inhibition be to prevent extensive metabolism of L-DOPA through *O*-methylation in the periphery. While both **1** and **2** recently reached the marketplace, **1** was subsequently withdrawn due to hepatotoxicity concerns,[13] leaving **2** as the sole COMT inhibitor presently available in the clinic for use as an adjunct to L-DOPA treatment of PD patients. Our concerns related to the rather short in vivo half-life of **2**, which implies a multiple and elevated daily dosage regime, led us to investigate the possibility of designing a potent, reversible, peripherally selective and long-acting COMT inhibitor and culminated in the discovery of BIA 3−202 **3**[14] (Figure 1), which is currently under clinical evaluation as an adjunct to L-DOPA treatment of PD.[15,16] This compound also bears the nitrocatechol motif, yet we were intrigued to find that homologation and structural

* Corresponding author. Tel: 351-22-9866100. Fax: 351-22-9866192. E-mail: psoares.silva@bial.com.
† Laboratory of Chemistry.
‡ Laboratory of Pharmacology.
§ Present Address: Institute of Pharmacology and Therapeutics, Faculty of Medicine, University of Oporto, 4200−319 Oporto, Portugal.

10.1021/jm040848o CCC: $27.50
Published on Web 11/02/2004

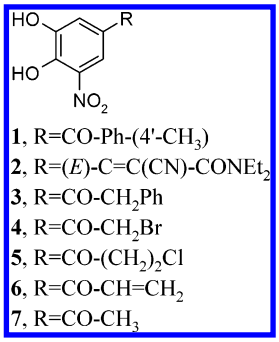

Figure 1. Chemical structures of tolcapone (**1**), entacapone (**2**), BIA 3-202 (**3**), and building blocks **4**−**7**.

variation of the hydrocarbon side-chain substituent of **3** resulted in highly significant effects on biological parameters, such as potency, duration, and selectivity of COMT inhibition. This prompted us to undertake the present study, principally investigating the effects of introducing homologous heteroatom-containing side-chain substitution (oxygen, nitrogen, and sulfur) to C-1 of the nitrocatechol pharmacophore, with the aim of ascertaining whether structural manipulations of the side chain could provide more structurally diverse COMT inhibitors possessing greater peripheral selectivity than **1** and increased duration of action compared to **2**.

Results and Discussion

The new COMT inhibitors herein presented were prepared using the readily accessible and suitably functionalized nitrocatechol building blocks **4**−**7** (Figure 1) as substrates for nucleophilic substitution, Michael addition, or Mannich reactions. Target compounds of general formula **I** with oxygen at the β-position relative to the carbonyl group of the side chain were easily prepared in generally moderate yields by reaction of the halo ketone **4** with appropriately substituted phenols or naphthols in the presence of weak base (K_2CO_3) in warm DMF (method A, Scheme 1). Derivatives of general formula **II** (n = 1) containing sulfur were synthesized by reaction either of **4** with substituted thiophenols under similar conditions as above (method B, Scheme 1), and the longer homologues (n = 2) were prepared smoothly via Michael addition to the α,β-unsaturated ketone **6** (method C, Scheme 1) again in reasonably good yields. Finally, reaction of **4** and **6** with selected secondary amines provided homologous compounds containing nitrogen in the side chain of general formula **III** (methods D and E, respectively, Scheme 1) in moderate to good yields, which were more easily isolated and purified as their hydrochloride salts. The Mannich reaction of the acetophenone **7** was exemplary in this respect (method E, Scheme 1), as the target compounds tended to precipitate toward the end of the reaction with excellent purity, thereby greatly facilitating isolation of the desired products by simple filtration.

Initially, high-throughput in vitro screening (human neuroblastoma SK-N-SH cells)[17] was used to test the ability of the new compounds to inhibit COMT, the results of which allowed construction of basic structure−activity relationships. Selected in vitro results of synthesized compounds are shown in Table 1 and are compared to **1** and **2**.

Scheme 1. Synthesis of Oxygen Containing Compounds I (Method A), Sulfur-Containing Compounds **II** (Methods B and C), and Nitrogen-Containing Compounds III (Methods D and E).

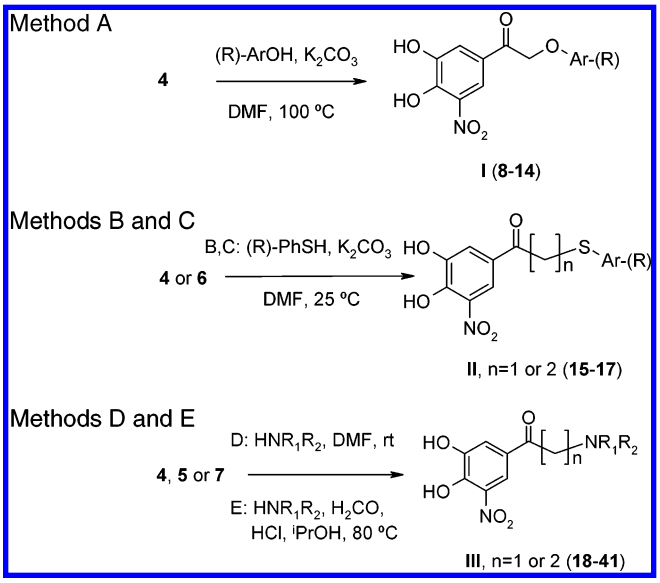

From the oxygen series, aryl compounds were certainly more active than **2** but less so than **1**. Incorporation of electron-donating (**9**, methoxyl) or electron-withdrawing groups (**11**, fluorine) made little difference. Interestingly, increasing the size of the aromatic ring had a noticeably positive effect on activity, and the more lipophilic analogues derived from either 1- or 2-naphthol (**12**−**14**) generally exhibited increased inhibition compared to their phenyl counterparts. In a similar vein to the oxygen analogues, sulfur-containing compounds showed slightly improved in vitro inhibition over **2**, but this activity was generally unaffected by homologation, as typified by **15** and **16**. Rather more interesting observations were made, however, in the nitrogen series. Initial results from compounds derived from small aliphatic secondary amines **18**−**21** were rather disappointing from the point of view of the relatively low in vitro inhibition but did serve to indicate that compounds with longer chains (n = 2) may be endowed with greater inherent activities than their lower homologues (n = 1). Indeed, this early hypothesis was in fact borne out, and similar general trends of increased in vitro inhibition were associated with the higher homologues of other classes of nitrogen-containing compounds, such as, for example, those derived from cyclic amines such as substituted piperidines **22** and **23**, thiomorpholines **24** and **25**, and substituted piperazines **26**−**42**. This latter class in particular displayed greatest early promise. Whereas the simple *N*-alkylpiperazines such as **26**−**29** were again relatively uninteresting, replacement of the substituent on the piperazine nitrogen with phenyl (**30**−**39**) or benzoyl groups (**40**−**41**) provided significant improvement, with the higher homologues (n = 2) now very significantly more active than **2** and essentially equipotent to **1**. Within this *N*-arylpiperazine series, incorporation of small alkyl substituents (**38**) or electron-withdrawing groups, such as halogen (**32**−**33**, **36**−**37**) or trifluoromethyl (**34**−**35**), were well-tolerated, but electron-donating groups such as methoxy (**39**) had quite the opposite effect.

Table 1. Percent Inhibition of COMT Activity in SK-N-SH Cells by Compounds **1**, **2**, and **8**−**41** (100 nM)[a]

Formula	No.	Substituent Ar-(R) for **I** and **II** NR_1NR_2 for **III**	% Inhibition	SEM	Method (Yield)	mp (°C)
	1		97	1		
	2		77	3		
I	**8**	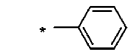	91	0	A (64%)	159-160
I	**9**	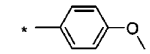	87	0	A (34%)	195-196
I	**10**	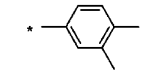	95	1	A (25%)	149-151
I	**11**	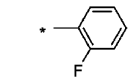	94	1	A (24%)	160-163
I	**12**	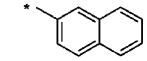	98	0	A (40%)	179-181
I	**13**	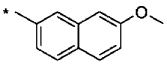	99	0	A (53%)	192-194
I	**14**	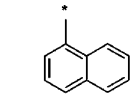	100	0	A (67%)	197-199
II, n=1	**15**	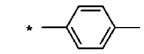	90	3	B (64%)	115-117
II, n=2	**16**	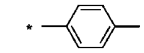	89	4	C (67%)	160-162
II, n=2	**17**	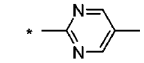	85	2	C (82%)	197-199
III, n=1	**18**	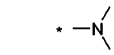	70	4	D (96%)	219-220
III, n=2	**19**	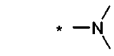	89	6	D (61%)	199-201
III, n=1	**20**	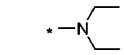	77	1	D (47%)	186-188
III, n=2	**21**	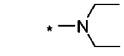	91	0	D (72%)	183-184
III, n=1	**22**	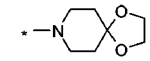	84	1	D (61%)	176-180
III, n=2	**23**	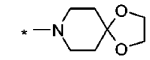	94	0	D (63%)	236-240
III, n=1	**24**	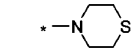	87	2	D (51%)	218-220
III, n=2	**25**	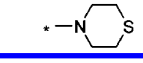	93	2	D (71%)	194-196
III, n=1	**26**	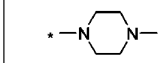	71	1	D (83%)	240(dec)
III, n=2	**27**	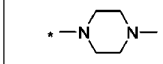	81	0	D (94%)	246-249
III, n=1	**28**	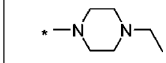	75	1	D (73%)	221-225
III, n=2	**29**	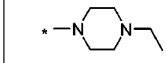	81	0	D (79%)	161-165
III, n=1	**30**	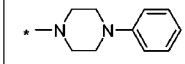	87	1	D (86%)	227-229
III, n=2	**31**	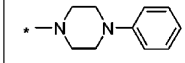	95	1	D (62%)	230-232
III, n=1	**32**	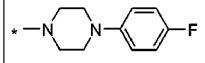	93	0	D (62%)	223-227
III, n=2	**33**	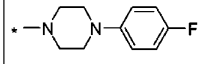	95	1	D (75%)	211-213
III, n=1	**34**	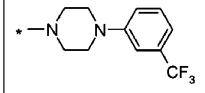	92	1	D (66%)	216-218
III, n=2	**35**	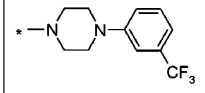	96	0	E (61%)	212-215
III, n=2	**36**	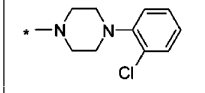	100	0	E (52%)	214-216
III, n=2	**37**	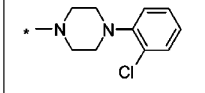	95	0	E (75%)	228-230
III, n=2	**38**	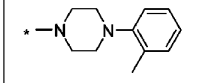	95	0	E (54%)	232-234
III, n=2	**39**	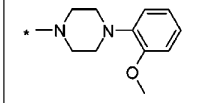	81	1	E (22%)	144-147
III, n=2	**40**	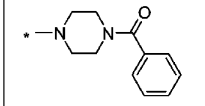	99	1	E (57%)	210-203
III, n=2	**41**	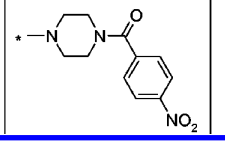	96	2	E (52%)	237-239

[a] Results are means ± SEM of four experiments per group. *Represents point of substituent attachment.

Having identified from this series two classes of nitrocatecholic compounds with novel side-chain substitution possessing potent in vitro COMT inhibitory activity, namely, the aryloxy and the *N*-arylpiperazine series, subsequent experiments were designed to evaluate both the duration of COMT inhibition and access to the brain of selected compounds from Table 1 and to compare them with the standards **1** and **2**. Test compounds were administered to overnight fasted mice, and thereafter, the animals were killed by decapitation at either one or 6 h after administration, whereupon the livers and brains were removed and used to determine COMT activity as previously described.[18] The time-course inhibition profiles are summarized in Table 2. Of the oxygenated compounds, **8** and particularly **9** displayed long-acting inhibition of peripheral COMT at 6 h but relatively lower selectivity than **2** at the shorter time point. However, **12** was significantly longer acting than **8**, **9**, and **2** and more selective at 1 h over regioisomer **14** and **2** itself. The sulfur compound **15** displayed an inhibition profile very similar to that of **2**. Of the nitrogen-containing compounds, the lower dialkylamines **20** and **21** again displayed relatively low activity, even at 1 h, whereas the *N*-benzoylpiperazine **40** displayed very high peripheral selectivity but very short duration of COMT inhibition. Of the *N*-arylpiperazine series, compound **35**, the 3′-trifluoromethylphenyl-substituted piperazine (Figure 2), clearly displayed the longest duration of COMT inhibition, retaining almost 75% inhibition, even at 6 h after oral adminis-

Table 2. Percent Inhibition of COMT Activity of Selected Compounds from Table 1 in Homogenates of Mouse Brain and Liver at 1 and 6 h after Administration (all at 30 mg/kg) by Gastric Tube[a]

	COMT activity at 1 h				COMT activity at 6 h			
	liver		brain		liver		brain	
no.	% inhibn	SEM	% inhibn	SEM	% inhibn	SEM	% inhibn	SEM
1	99	1	99	1	94	1	86	8
2	76	4	23	10	26	8	15	8
8	78	4	39	4	50	9	−4	6
9	71	1	41	6	65	6	7	9
12	83	3	17	5	61	5	−19	13
14	86	2	37	5	69	6	8	11
15	70	2	20	10	23	15	−15	7
20	50	2	22	16	33	9	−11	12
21	62	3	26	12	43	5	−26	8
25	70	4	7	19	42	9	−7	3
34	50	3	24	9	53	3	0	10
35	82	7	14	14	74	4	14	11
36	46	7	6	3	28	0	4	18
40	84	4	13	8	18	5	−22	4

[a] Results are means ± SEM of four experiments per group

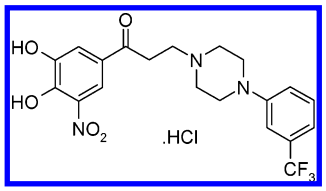

Figure 2. Chemical structure of **35** (BIA 3-335).

tration, compared to only 25% for **2**. Additionally, **35** exhibited far superior selectivity than **1** at both time points for peripheral over central COMT inhibition.

In an effort to rationalize these results obtained from both the in vitro and in vivo studies, we resorted to application of a combination of molecular modeling and computational methods with the 3-fold intention of analyzing and reviewing the structure of the COMT in complex with **35**, explaining the structure−activity relationships observed within this novel series of inhibitors, and justifying the poor blood−brain permeability of **35**.

The structure of the ternary complex between recombinant rat liver COMT, the cosubstrate SAM, and the inhibitor **35** has been determined by X-ray crystallography,[19,20] and a discussion of the interactions at the atomic level has been reported[20] (indeed, this is the first 3D structure determination of COMT complexed with a potentially therapeutically useful inhibitor). Briefly, the nitrocatechol is responsible for "anchoring" the inhibitor to the enzyme, via hydrogen-bonding to Glu199 and Lys144 and through coordination of the magnesium ion in the catalytic site. In contrast, the propanone, piperazine, and trifluoromethylphenyl moieties of **35** extend out from the narrow catalytic pocket, flanked by Trp38, Pro174, and Leu198, and form hydrophobic interactions along a shallow groove at the surface of the protein. Due to the lack of hydrogen bonds or tight steric restrictions, the bound conformation of the inhibitor's side chain groups appears to be loosely determined, as indicated by the corresponding high average thermal factors observed (B_{avg} of 45.1 and 55.7 A^2 for the piperazine and trifluoromethylphenyl moieties, respectively).

To quantify and characterize the nature of the intermolecular interactions responsible for its high stability, the protein−ligand complex was reexamined. One of the major difficulties in evaluating and scoring intermolecular interactions is the adequate treatment of entropic terms associated with the desolvation processes that occur upon complex formation. Such desolvation terms are especially important for interactions that are dominated by hydrophobic contacts, as in the present case of COMT and the long side chain of **35**.

The HINT algorithm utilizes a fragmentation process to assign atom-based hydrophatic constants, based on experimentally determined solvent partition log *P* values between water and octanol. The atom−atom interaction function is based on the relative hydrophatic constants, and the strength of an intermolecular association is computed over the sum of atom−atom scores. Since the parameter log *P* is a thermodynamic constant associated with the free energy of solvent transfer, both enthalpic (van der Waals, hydrogen-bonding, Coulombic interactions) and entropic (solvation, "hydrophobic interactions") terms are treated implicitly by this empirically based function. A correlation between HINT hydrophatic scores and the free energy of binding of 53 protein−ligand complexes has been recently suggested.[21]

Of relevance to the intermolecular interactions are the actual protonation states of the nitrogen atoms of the piperazine ring of **35**. Since experimentally determined ionization constants for **35** were unavailable, the piperazinyl nitrogen atoms were instead computed using the ACD/pK_a fragmental method (Advanced Chemistry Development, Inc) and found to have pK_a values below 6.0. One piperazinyl nitrogen atom is linked to a trifluoromethyl-substituted phenyl ring and is therefore expected to be neutral. Although the second nitrogen is indirectly connected to the carbonyl and nitrocatechol moieties, these groups appear to have an inductive effect through the aliphatic spacer, thereby lowering the pK_a of this nitrogen atom. Therefore, the piperazine was considered to be unprotonated at physiological pH and modeled as such in subsequent studies.

The hydrophatic interactions between **35** and COMT within the complex were calculated using the HINT scoring function, as detailed in the methods. Figure 3a shows isocontour surfaces representing favorable intermolecular hydrophobic interactions. Polar interactions are mostly confined to the catechol-binding region and are not shown. Apart from the strong electrostatic and hydrogen-bonding interactions of the catechol moiety, the so-called "gatekeepers" Pro174, Trp38, and Leu198 are responsible for most of the hydrophobic stabilizing interactions. Also Trp143 and Met40 establish important van der Waals contacts with the nitrocatechol group. Most notably, the terminal trifluoromethylphenyl group points away from the protein surface (atoms colored cyan) and makes only weak van der Waals contacts (Figure 3a, green surface) with Trp38 and Met201. Such a bound conformation is somewhat unexpected in a solvated complex, since the hydrophobic trifluoromethylphenyl group would remain extensively solvated. Interestingly, however, if crystallographic neighboring molecules are generated using the symmetry operations of the crystallographic space group $P3_221$, it can be seen that the piperazine and trifluoromethylphenyl moieties of the inhibitor, as well as few

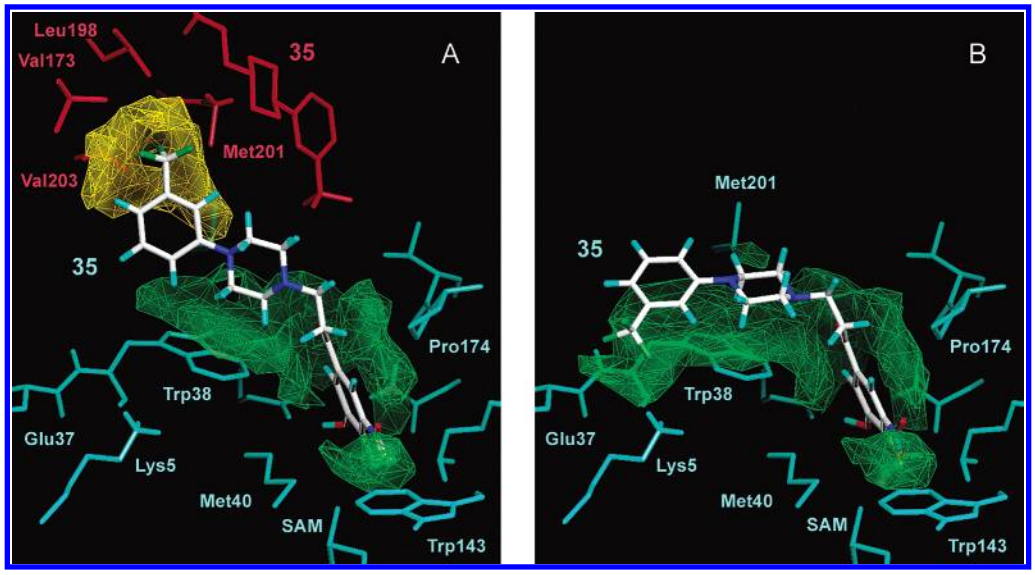

Figure 3. HINT interaction maps showing favorable hydrophobic contacts between COMT and **35**. (A) Structure of the crystallographic complex 1H1D showing the inhibitor (color scheme according to element type: carbon, white; hydrogen, cyan; oxygen, red; nitrogen, blue; fluorine, green) complexed with COMT (cyan). A symmetry-related, closely interacting molecular complex that is present in the crystal framework is shown in red. Green and yellow isocontour surfaces define favorable hydrophobic interactions between **35** and the single protein chain (intracomplex) or with the nearest complex structure within the crystal, respectively. (B) Structure of the lowest energy binding mode of the inhibitor in complex with COMT, obtained by docking. Interaction isocontour surfaces are plotted at the same energy level in both panels.

vicinal residues, form close van der Waals contacts with a symmetrically positioned complex molecule (Figure 3a, red atoms). In particular, the trifluoromethylphenyl group interacts closely (Figure 3a, yellow surface) with the side chains of a cluster of hydrophobic residues of the second COMT monomer, comprised by Val173, Leu198, Met201, and Val203. Such interactions would be absent under physiological conditions, where COMT functions exclusively as a monomeric protein. The above observation raises the hypothesis that the terminal side chain groups (piperazine and trifluoromethylphenyl) of **35** are stabilized in an alternative conformation, induced by a vicinal complex structure present in the crystal form and that the observed conformation may not be representative of the actual complex formed in solution.

To further assess this hypothesis, we first explored alternative binding conformations of **35** with the structure of one monomer of COMT using molecular docking simulations. Docking was performed with the program GOLD, which uses a genetic algorithm to optimize the conformation of the bound inhibitor. Fifty independent docking runs, followed by local energy minimization, were performed (starting from random configurations) to ensure a wide exploration of the configurational landscape of interaction. During docking simulations, the coordination bonds between the Mg^{2+} ion and the catechol hydroxyl groups are implicitly treated as special hydrogen bonds, where the metal behaves as a hydrogen-bond donor. This enables adequate binding geometries to be found without imposing any additional constraints, although the energetics of the coordination bonds are likely to be Hill-estimated. However, the relative coordinates of the catechol moieties are virtually identical in all of the docked structures, so the errors are expected to be fairly constant, allowing direct comparisons to be made.

Finally, the hydrophatic interactions were computed for all alternative poses and compared to the binding energetics of the crystallographic complex, with and without considering the presence of the second protein monomer. It must be pointed out that HINT potential functions also lack parameters for metal coordination complexes, and therefore, the (important) contribution of the coordination bonds to the overall interaction energetics of the complexes is currently ignored. However, the same reasoning indicated above may apply and comparison between different poses should still be valid.

Figure 4a plots the hydrophatic interaction scores of inhibitor **35** in each of 50 putative binding modes against the corresponding root-mean-square (rms) deviations from the crystallographic structure. Visual inspection of the independently docked poses reveals three main families of conformationally related structures, with rms deviations from the experimental structure ranging from 1.0 to 3.7 Å. In particular, the position of the nitrocatechol and the propanone carbonyl groups were accurately predicted, but the conformation of the two side-chain rings of the inhibitor molecule could not be equally well reproduced in any of the docked solutions. Structurally, they differ from that of the crystallographic complex by a dihedral torsion of the propanone side chain as well as different rotations of the terminal trifluoromethylphenyl group (Figure 4b). However, such conformational adjustments predicted by docking enable a better stacking of the piperazine motif and, additionally, in the case of structure III, of the trifluoromethylphenyl moiety over Trp38.

In terms of interaction energetics, any of the three predicted binding modes could represent a more stable complex than that observed in the crystallographic complex between **35** and one monomer of COMT (HINT score $\times 1 = -1641.0$). The additional stabilizing energy is mostly attributed to an optimization of the hydrophobic contacts between the two molecules. In particular, the lowest energy binding mode (structure cluster III in Figure 4) enables the stacking of the trifluorom-

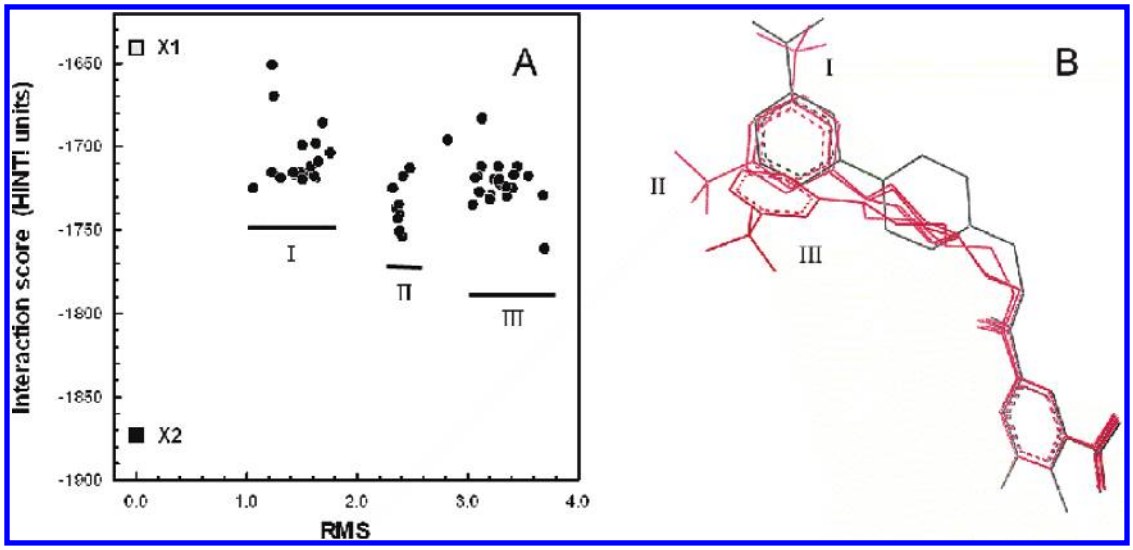

Figure 4. Docking results between COMT and compound **35**. (A) Hydrophatic interaction scores calculated for each of the 50 putative binding modes versus the corresponding rms deviations from the crystallographic structure of the complex. ×1, interaction score between **35** and one single chain of COMT in the crystal structure; ×2, interaction score calculated including the coordinates of the nearest symmetry-related molecular complex in the crystal (see the text). (B) Three alternative bound conformations of **35** (red) superimposed on the atomic coordinates (black) of the crystallographic complex (protein not shown).

ethylphenyl ring onto Trp38, consequently excluding water molecules from hydrophobic surfaces. Figure 3b shows the favorable hydrophobic interaction maps between COMT (single chain) and **35** in the lowest energy conformation predicted by docking. Comparison of this interaction map to that of the crystallographic complex (Figure 3a) clearly reveals additional hydrophobic contacts between **35** and Trp38 that contribute to a more negative (more favorable) hydrophatic interaction score (HINT score III = −1761.0), while the interactions made by the nitrocatechol or the propanone moieties are essentially unchanged.

Most notably, under the particular crystallization conditions, the trifluoromethylphenyl group is not in fact exposed to the solvent, as suggested by the isolated complex structure. Instead, it forms extensive van der Waals contacts with a cluster of hydrophobic residues of a crystallographic neighboring complex, as discussed above. The side chains of Val173, Leu198, Met201, Val203 and a second inhibitor molecule belonging to this symmetrically positioned complex form a hydrophobic pocket that shields the nonpolar trifluoromethylphenyl group from the solvent. Such intercomplex molecular interactions, depicted in Figure 3a (yellow surface), contribute largely to the stabilization of the crystallographic conformation of the inhibitor. If the coordinates of the neighboring molecule are also included in the calculations, the hydrophatic interaction energy of **35** becomes significantly more negative (HINT score ×2 = −1873.0) than that estimated for the isolated complex or for any of the docked models (Figure 4a).

In summary, the present results suggest that the bound conformation of **35**, as observed in the crystal structure of the complex, may indeed represent a stable configuration within the framework of the crystal. However, it is proposed that this particular binding conformation could be induced by the crystallization conditions due to nonphysiological interactions between symmetry-related molecules in the crystal and, consequently, may not be representative of the actual complex in solution. An alternative, hypothetical structure of the actual complex in solution is herein proposed (Figure 3b), based on docking simulations and hydrophatic interaction calculations. In this model, the piperazine and trifluoromethylphenyl moieties of **35** adopt a stacking conformation over Trp38, which enables better solvent exclusion from hydrophobic regions and consequently an additional intermolecular stabilizing energy. At the opposite end, the nitrocatechol fits into the catalytic pocket, exactly in the same manner as for the crystallographic complexes of **35**[20] and 3,5-dinitrocatechol,[22] forming coordination bonds to the magnesium ion and two hydrogen bonds to Lys144 and Glu199. Extensive van der Waals contacts with Trp38, Met40, Trp143, Pro174, and Leu198 also contribute significantly to the stabilization of the complex.

With regard to analysis of structure−activity within this novel series, observed in vitro inhibition showed a consistent dependency on side chain homologation, with longer chains ($n = 2$) endowing greater inherent activities than their lower homologues ($n = 1$). To understand the nature of this effect, the conformational spaces accessible to each pair of homologues ($n = 1$ or 2), within the active site of COMT, were compared by flexible docking simulations again using GOLD. Results are exemplified with the case of homologues containing the small aliphatic amine side chain, **18** and **19**, which are the simplest nitrogen-containing compounds of the series but which also show the highest dependency on homologation. Nevertheless, the same general conclusions can be extended to the other series of homologues tested.

As already discussed, the nitrocatechol pharmacophore, as well as the propanone carbonyl function, fits inside the narrow catalytic site of COMT, which is flanked by Trp38, Pro174, and Leu198. On the other hand, the rest of the side chain extends out of the catalytic pocket and interacts loosely with the protein surface. In the case of lower homologues ($n = 1$), the shorter (dimethylamino)ethanone chain is sterically constrained by Trp38 and Pro174 residues (Figure 5a), thereby conferring only limited conformational flex-

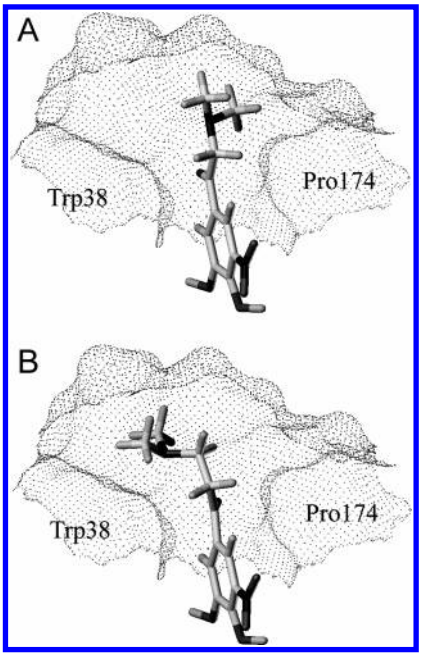

Figure 5. Illustrative structures of docked configurations of homologues **18** (panel A) and **19** (panel B). The partial shape of the catalytic pocket and surrounding protein surface is also shown.

ibility to the dimethylamine function. As a result, both terminal methyl groups are forced into the solvent, making only suboptimal contacts with the protein surface. Conversely, the homologation of the ethanone chain by a single methylene group confers a much wider configurational landscape to the side chain in the bound state. With the longer propanone spacer extending out of the narrow pocket entrance, the dimethylamine group becomes free to rotate about the external C−C bond of the propanone. Our docking results (not shown) indicate that, due to such conformational topology, the dimethylamine group is able to stack on top of the hydrophobic Trp38 side chain, therefore minimizing the solvent exposure of the two methyl groups, as illustrated in Figure 5b. This more favorable interaction may also compensate for the increased loss of entropy upon association. Similar behavior was observed for homologous cyclic amines such as the substituted piperidines **22** and **23**, thiomorpholines **24** and **25**, and the substituted piperazines **26**−**35**, where the van der Waals interactions of the ring systems can be systematically optimized in the case of the higher homologues. The results herein discussed suggest that steric constraints caused by Trp38 and Pro174 prevent optimization of hydrophatic interactions of the shorter homologues with the protein surface, thereby explaining the increased activity for the higher homologues.

It is also interesting to note that, within the series of equivalent homologues containing a piperazine motif, the in vitro data indicates that replacement of a small alkyl substituent (**26**−**29**) on the piperazine nitrogen with a phenyl or a nonpolar substituted phenyl group (**30**−**38**) results in a significant increase in inhibition. Given the predominantly hydrophobic nature of the protein surface surrounding the catalytic site and in light of the discussion above, it is herein suggested that this increased potency results from more favorable and extended hydrophatic interactions between the enzyme and the larger hydrophobic side chain of the ligand. Within the piperazine compounds, the same pattern of higher activities observed for the higher homologues due to optimization of binding configurations could again be explained as discussed above.

Finally, we studied the blood−brain barrier permeation of **35**. The entry of a drug into the brain is a complex process, which depends on multiple factors. Binding to plasma proteins, passive diffusion across the BBB, differential metabolism, and active efflux from the CNS may all contribute to a drug's partitioning from blood into the brain. It is known from practice that lipophilicity and H-bonding capacity influence to some extent the passive diffusion of drugs across the BBB. Molecular size, flexibility, polarity, and electrostatics are other properties that are thought to influence membrane partition, and since biological membranes are anisotropic systems, the three-dimensional distribution of such molecular determinants must also be considered important.

We applied a computational approach to study the structural factors determinant for the observed selectivity of **35** for peripheral COMT inhibition. A set of 72 molecular determinants relevant to the process of membrane partitioning was computed with the software VOLSURF as detailed in the methods and projected onto a predictive model of BBB permeation. This model, which was developed elsewhere,[23] correlated the same set of descriptors with the experimentally obtained permeation of nearly 300 known drugs and was able to correctly assign the BBB behavior for more than 90% of the compounds. Compounds computed to have positive scores are predicted to partition into the membrane (BBB+), whereas those with negative scores (BBB−) will have reduced probability of crossing the BBB by passive diffusion. Near-zero scores may indicate compounds with borderline or dubious behavior. The average scores for nearly 300 drugs in the training and validation sets are +0.5 for compounds showing BBB+ behavior and −0.6 for the BBB− drugs.

From the results herein obtained, **35** is predicted to behave as a moderate BBB− compound (BBB score = −0.7), which is in good agreement with the observed selectivity for peripheral COMT inhibition. It must be pointed out that the current model is based on a discriminant PLS procedure that aims solely at classifying a given compound in either the BBB+ or BBB− categories but does not necessarily permit prediction of the diffusion rate across the membrane system.

It is informative to analyze how the partitioning behavior is influenced by the individual molecular determinants. Figure 6a plots the variable weights for the first and most significant component of the BBB model. The vertical bars represent the relative contributions of each individual molecular descriptor to the global BBB score. A detailed discussion of such contributions is presented elsewhere,[23] but a brief summary of the most relevant characteristics is given below to ease the interpretation of our results. Positive bars indicate descriptors whose values are directly proportional to membrane permeability, while descriptors with negative bars show an inverse correlation with permeation. It can be seen from this plot that BBB permeability decreases with an increase of the compound's

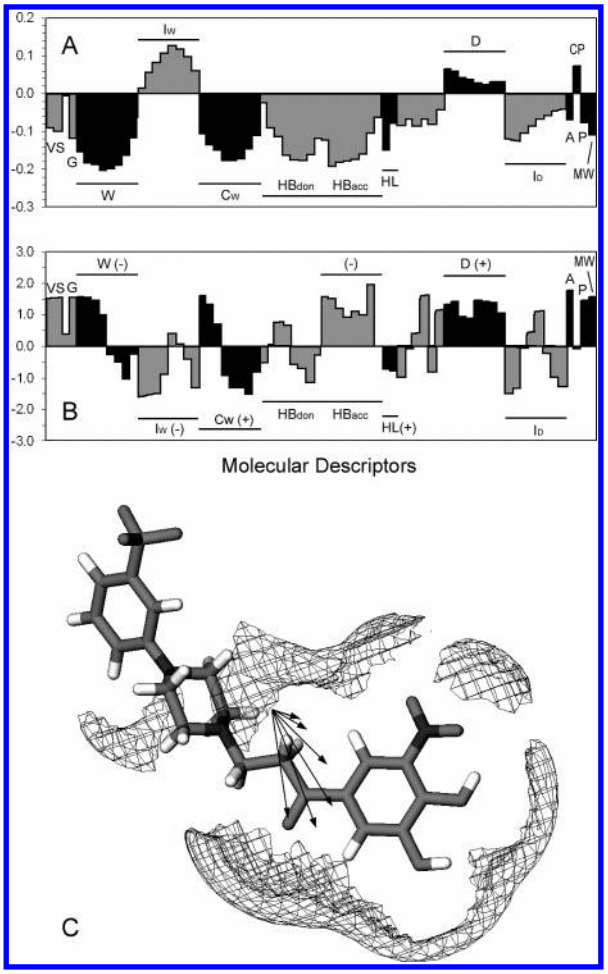

Figure 6. Volsurf descriptors of BBB model. (A) PLS weights plot for the first and most significant component of the blood−brain permeation model. Vertical bars represent the relative contributions of each of the 72 individual molecular descriptors to the global BBB score. Positive bars indicate descriptors whose values are directly proportional to membrane permeability while descriptors with negative bars show an inverse correlation with permeation. Different shades help differentiating groups of descriptors. *V*, volume; *S*, surface; *G*, globularity; *W*, hydrophilic regions; I_W, hydrophilic integy moments; C_W, hydrophilic capacity factors; HB, hydrogen-bonding; HL, hydrophilic−lipophilic balance; *D*, hydrophobic regions; I_D, hydrophobic integy moments; *A*, amphiphilic moment; *P*, polarizability; MW: molecular weight. (B) Profile of molecular descriptors computed for **35**. The original values were scaled to unit variance and centered on the average value of each descriptor. (C) Hydrophilic molecular interaction fields of **35** calculated with a water probe. The surfaces shown represent regions contoured at −3 kcal/mol.

H-bonding (HB descriptors) potential, the extent of hydrophilic regions (*W* descriptors), and the hydrophilic capacity factors (C_W descriptors). The three-dimensional distribution, as well as the number, of polar or hydrogen-bonding groups in the molecule is very important. The negative weights associated with the capacity factors, which relate to hydrophilic interactions per surface unit, indicate that dense and localized polar regions tend to hinder partitioning into the membrane, whereas weak or diffuse polar surfaces are better tolerated. Moreover, the greater the off-set between the barycenter of the hydrophilic regions and the center of mass of the molecule, i.e., the hydrophilic *integy* moment (I_W descriptors), the more likely a compound is to cross the BBB. On the other hand, descriptors of hydrophobic interactions (*D*) are directly correlated with BBB permeability, especially if evenly distributed along the molecular surface, as indicated by the negative weights associated with the hydrophobic *integy* moments (I_D descriptors).

Figure 6b shows the profile of molecular descriptors computed for **35**. The original values were scaled to unit variance and centered on the average value of each descriptor. Positive or negative values consequently indicate molecular determinants with values above or below the population's average, respectively. The low BBB permeability of **35** can be generally explained by the combined effects of four major classes of molecular determinants. The presence of two catechol hydroxyl groups, along with the solvent accessible carbonyl function and two piperazinyl nitrogen atoms, provides an extended hydrophilic surface (*W*, Figure 6b,c), which contributes to limiting membrane partitioning. The detrimental contribution of such hydrophilic potentials to BBB permeability is only slightly mitigated by the fact that they are diffusely distributed along large areas of the molecular surface, as indicated by the net negative capacity factors (C_W). Moreover, hydrogen-bonding potential, namely the high content of hydrogen-bond acceptor functions, also contributes negatively to the diffusion of **35** through the membrane system.

The anisotropy of distribution of hydrophilic regions along the molecular axis (hydrophilic integy moments, I_W) generally correlates directly with BBB permeability. However, in the case of **35**, the hydrophilic regions distribute evenly along most of the molecular axis, with the exception of the terminal trifluoromethylphenyl group. In particular, the presence of the hydrophilic piperazinyl, which is "separated" from the polar nitrocatechol moiety by the 1-propanone chain, contributes to a reduction in the hydrophilic integy moments, therefore limiting the ability to partition into the BBB. Other molecular determinants of **35** that contribute to poor permeability are the large molecular volume (*V*) and surface (*S*), polarizability (*P*), and elongated shape (*G*), which is also related to molecular flexibility. On the other hand, the descriptors related to hydrophobic regions are all above average, which correlates positively, though weakly, with a BBB+ behavior. The inclusion of a polar group at the terminal (trifluoromethyl)phenyl moiety of the molecule could have the effect of decreasing the hydrophobicity as well as the hydrophilic integy moments, potentially contributing to lowering the partitioning of the compound between aqueous and membrane phases.

Conclusions

A novel series of COMT inhibitors containing the nitrocatechol pharmacophore has been prepared. The introduction and nature of heteroatom-containing substituents were found to have a most profound effect on both the peripheral selectivity and duration of COMT inhibition. Compounds containing oxygen in the side chain such as **12** and **14** were identified as highly potent in vitro inhibitors and subsequently as long-acting and reasonably selective inhibitors of peripheral COMT in vivo. However, from the series of highly in vitro active *N*-arylpiperazine inhibitors, 1-(3,4-dihydroxy-5-nitro-

phenyl)-3-[4-[3-(trifluoromethyl)phenyl]-1-piperazinyl]-1-propanone hydrochloride (**35**, BIA 3−335) was found to exhibit potent and almost completely peripherally selective COMT inhibition in the mouse, unlike the nonselective inhibitor tolcapone **1**, and is endowed with significantly improved duration of action compared to entacapone **2**. Molecular modeling was utilized to gain an understanding of the basic structure−activity relationships within this novel series and has also provided fresh insight into the structure of the ternary complex formed between COMT and **35**. Furthermore, computational analysis was successfully applied to the identification of the molecular determinants responsible for the low BBB permeability of **35**, which in effect proportions excellent peripheral selectivity on this compound. Accordingly, **35** is presented as a promising candidate for clinical evaluation as an adjunct to L-DOPA therapy for the treatment of Parkinson's disease.

Experimental Section

Chemistry. Melting points were measured in open capillary tubes on an Electrothermal Model 9100 hot stage apparatus and are uncorrected. NMR spectra were recorded on a Bruker Avance DPX (400 MHz) spectrometer with solvent used as internal standard, and data are reported in the order: chemical shift (ppm), number of protons, multiplicity (s, singlet; d, doublet; t, triplet; q, quartet; m, multiplet; br, broad), approximate coupling constant (*J*) in hertz, and assignment of a signal. IR spectra were measured with a Bomem Hartmann & Braun MB Series FTIR spectrometer using KBr disks. Analytical TLC was performed on precoated silica gel plates (Merck 60 Kieselgel F 254) and visualized with UV light. Elemental analyses were performed on a Fisons EA 1110 CHNS instrument, and all analyses are consistent with theoretical values to within ±0.4%, unless otherwise indicated. Solvents and reagents were purchased from Aldrich, Merck, Fluka and used as received unless otherwise noted.

Building blocks **4** and **7** are known compounds,[24] and **5** can be prepared in three steps by standard procedures from 2-methoxyphenol via Friedel−Crafts acylation (chloropropionyl chloride, $AlCl_3$), nitration (60% HNO_3 in AcOH), and demethylation ($AlCl_3$, $Cl(CH_2)_2Cl$, Δ). The unsaturated ketone **6** was isolated in 87% yield from the reaction of **5** with potassium phenolate in warm DMF (1 h at 100 °C). The following details are representative procedures for synthesis of compounds **8**−**41**.

Method A: 1-(3,4-Dihydroxy-5-nitrophenyl)-2-(1-naphthalenyloxy)ethanone 14. To a stirred solution of 1-naphthol (1.54 g, 10.69 mmol) in DMF (10 mL) at room temperature was added powdered potassium carbonate (1.48 g, 10.69 mmol) in one portion followed by 2′-bromo-1-(3,4-dihydroxy-5-nitrophenyl)ethanone **4**, (0.75 g, 2.72 mmol). The resulting deep red suspension was then stirred at 100 °C for 1 h and then allowed to cool to room temperature. The inorganic material was removed by filtration and the filter cake was washed with DMF (5 mL). The combined filtrate was then evaporated (Labconco Centrivap Concentrator, 75 °C), and water (15 mL) was added to the dark residue. The mixture was extracted by ethyl acetate (2 × 20 mL), and the organic extracts were washed by water (10 mL) and brine (10 mL) and then dried over anhydrous sodium sulfate, filtered, and evaporated (40 °C, water aspirator pressure) to leave an orange-brown solid. Recrystallization from acetic acid afforded yellow-orange crystals (0.62 g, 67%): ν_{max} (KBr disk)/cm^{-1} 3376 (OH), 1699 (CO), and 1545 (NO_2); δ_H (400 MHz, DMSO-d_6) 11.05 (2 H, br, 3-OH, 4-OH), 8.31−8.25 (2 H, m, Ph), 8.22 (1 H, d, *J* 2.1, H-6), 8.15−7.85 (2 H, m, Ph), 7.60 (1 H, d, *J* 2.1, H-2), 7.52−6.97 (3 H, m, Ph), and 5.70 (2 H, s, CH_2); δ_C (100 MHz, DMSO-d_6) 193.01, 154.29, 148.82, 147.11, 138.34, 135.14, 128.51, 127.56, 127.02, 126.41, 125.91, 125.77, 122.73, 121.42, 117.90, 117.21, 106.83, and 71.21. Anal. ($C_{18}H_{13}NO_6$) C, H, N.

Method B: 1-(3,4-Dihydroxy-5-nitrophenyl)-2-[(4-methylphenyl)thio]ethanone 15. To a stirred solution of 4-thiocresol (0.19 g, 1.49 mmol) in DMF (4 mL) at room temperature was added powdered potassium carbonate in one portion followed by α-bromo ketone **4** (0.41 g, 1.49 mmol) in three portions. The resulting suspension was stirred for 20 min and then filtered, and the filter cake was washed by DMF (1 mL). The combined filtrate was evaporated (Labconco Centrivap Concentrator, 75 °C) and water (5 mL) was added to the residue. The mixture was extracted by ethyl acetate (2 × 15 mL), and the organic extracts were washed by dilute hydrochloric acid (10 mL), water (10 mL), and brine (10 mL); dried over anhydrous sodium sulfate; filtered; and evaporated (40 °C, water aspirator pressure) to leave a pale yellow oil that solidified on standing. Recrystallization from acetic acid afforded yellow crystals (0.304 g, 64%): ν_{max} (KBr disk)/cm^{-1} 3369 (OH), 1684 (CO), and 1539 (NO_2); δ_H (400 MHz, DMSO-d_6) 10.90 (2 H, br, 3-OH, 4-OH), 8.01 (1 H, d, *J* 2.1, H-6), 7.62 (1 H, d, *J* 2.1, H-2), 7.22 (2 H, d, *J* 7.9, Ph), 7.10 (2 H, d, *J* 8.2, Ph), 4.51 (2 H, s, CH_2), and 2.30 (3 H, s, OCH_3); δ_C (100 MHz, DMSO-d_6) 192.91, 148.64, 147.07, 138.21, 137.07, 132.30, 130.74, 130.52, 126.51, 118.47, 117.90, 40.91, and 21.60. Anal. ($C_{15}H_{13}NO_5S$) C, H, N.

Method C: 1-(3,4-Dihydroxy-5-nitrophenyl)-3-[(4-methylphenyl)thio]-1-propanone 16. To a stirred solution of 4-thiocresol (0.071 g, 0.57 mmol) in DMF (4 mL) at room temperature was added powdered potassium carbonate in one portion followed by 1-(3,4-dihydroxy-5-nitrophenyl)-2-propen-1-one **6** (0.1 g, 0.48 mmol) in one portion. The resulting suspension was stirred for 20 min and then filtered, and the filter cake was washed by DMF (1 mL). The combined filtrate was evaporated (Labconco Centrivap Concentrator, 75 °C) and water (5 mL) was added to the residue. The mixture was extracted by ethyl acetate (2 × 15 mL), and the organic extracts were washed by dilute hydrochloric acid (10 mL), water (10 mL) and brine (10 mL); dried over anhydrous sodium sulfate; filtered; and evaporated (40 °C, water aspirator pressure) to leave an orange-brown solid. Recrystallization from acetic acid afforded orange crystals (0.11 g, 67%): ν_{max} (KBr disk)/cm^{-1} 3377 (OH), 1689 (C=O), and 1542 (NO_2); δ_H (400 MHz, DMSO-d_6) 10.86 (2 H, br, 3-OH, 4-OH), 7.97 (1 H, d, *J* 2.1, H-6), 7.52 (1 H, d, *J* 2.1, H-2), 7.21 (2 H, d, *J* 8.2, Ph), 7.10 (2 H, d, *J* 8.2, Ph), 3.31 (2 H, t, CH_2), 3.26 (2 H, t, CH_2), and 2.34 (3 H, s, CH_3); δ_C (100 MHz, DMSO-d_6) 196.51, 148.65, 146.89, 138.10, 136.51, 133.24, 130.81, 129.96, 127.71, 117.93, 117.01, 38.30, 28.50, and 21.51. Anal. ($C_{16}H_{15}NO_6S$) C, H, N.

Method D: 1-(3,4-Dihydroxy-5-nitrophenyl)-2-(dimethylamino)ethanone Hydrochloride 18. To a stirred solution of α-bromo ketone **4** (0.1 g, 0.36 mmol) in DMF (4 mL) at room temperature was added a 40% aqueous solution of diethylamine (0.43 mL, 3.46 mmol), and the resulting deep red solution was stirred for 1 h, causing formation of a dark orange precipitate. The solvent was removed by evaporation (Labconco Centrivap Concentrator, 75 °C) and ethanol (2 mL) was added to the residue, which was acidified to pH 1 by the addition of a few drops of concentrated hydrochloric acid. On standing, a precipitate formed which was removed by filtration and washed with ethanol (1 mL) to give, after drying, a yellow solid (0.096 g, 96%): ν_{max} (KBr disk)/cm^{-1} 3265 (OH), 1688 (C=O), and 1548 (NO_2); δ_H (400 MHz, DMSO-d_6) 11.22 (1 H, br, 4-OH), 10.12 (1 H, br, 3-OH), 8.04 (1 H, d, *J* 2.1, H-6), 7.76 (1 H, d, *J* 2.1, H-2), 5.02 (2 H, s, CH_2), and 2.91 (6 H, s, 2 × CH_3); δ_C (100 MHz, DMSO-d_6) 190.22, 149.33, 148.37, 138.15, 124.73, 117.32, 62.34, and 44.72. Anal. ($C_{10}H_{12}N_2O_5.HCl{\cdot}0.5H_2O$) C, H, N.

Method E: 1-(3,4-Dihydroxy-5-nitrophenyl)-3-[4-[3-(trifluoromethyl)phenyl]-1-piperazinyl]-1-propanone Hydrochloride 35. To a stirred suspension of 3,4-dihydroxy-5-nitroacetophenone **7** (0.2 g, 1.01 mmol) in 2-propanol (5 mL) at room temperature was added 1-(α,α,α-trifluoro-*m*-tolyl)-piperazine (0.29 g, 1.28 mmol) followed by a 35% aqueous solution of formaldehyde (0.5 mL) and concentrated hydrochloric acid (0.42 mL, 5.07 mmol). The mixture was then stirred and heated at reflux for 7 h, during which time a

copious yellow precipitate formed. The mixture was allowed to cool to room temperature and the solid was filtered off and washed with 2-propanol (1 mL). After drying, there was obtained a yellow solid (0.27 g, 61%): ν_{max} (KBr disk)/cm^{-1} 3415 (OH), 1688 (C=O), and 1548 (NO_2); δ_H (400 MHz, DMSO-d_6) 10.90 (2 H, br, 4-OH, 3-OH), 8.13 (1 H, d, *J* 2.1, H-6), 7.73 (1 H, d, *J* 2.1, H-2), 7.51 (2 H, t, *J* 7.9, Ph), 7.33 (2 H, m, Ph), 3.64 (2 H, t, $COCH_2$), 3.51 (2 H, t, CH_2), and 3.35−3.22 (8 H, m, 4 × CH_2); δ_C (100 MHz, DMSO-d_6) 195.11, 150.96, 148.98, 147.34, 138.22, 131.27, 130.99, 127.22, 125.01, 120.35, 117.86, 117.41, 116.83 (m), 112.81 (m), 51.86, 51.72, 45.91, and 33.45. Anal. ($C_{20}H_{20}F_3N_3O_5$.HCl·0.75H_2O) C, H, N.

Pharmacology. Complete experimental protocols for the evaluation of in vitro and in vivo COMT inhibitory activity of new compounds have been previously reported.[14,17−18] All animal interventions were performed in accordance with European Directive number 86/609 and the rules of the National Institute of Health's *Guide for the Care and Use of Laboratory Animals* (http://oacu.od.nih.gov/regs/guide/guidex.htm).

Computational Methods. Preparation of Molecular Structures. Atomic coordinates of the ternary complex between COMT, the cosubstrate SAM, and the inhibitor **35** (BIA 3−335) were obtained from the PDB file 1H1D.[19,20] Nearest symmetry-related molecules were generated with the symmetry operations of the crystallographic space group *P*321 using the program Swiss-Pdb Viewer.[25] For all subsequent molecular modeling operations, the crystallographic water molecules were deleted (except HOH53 coordinated to Mg^{2+}) and all hydrogen atoms were added to the ligands and protein atoms, using standard procedures. Due to the vicinity of the Mg^{2+} ion and the positively charged SAM moiety, the catalytic Lys144 residue is suggested to have an exceptionally lowered pK_a.[26,27] Therefore, the side chain NH_2 function of Lys144 was modeled in the neutral form. Hydrogen atoms in the crystallographic structure were finally optimized by energy minimization and intermolecular hydrogen bonds were checked for optimal geometry.

Molecular Docking. Unrestrained flexible docking between COMT and selected inhibitors was performed with the program GOLD version 1.2[28−30] using a genetic optimization algorithm. Default parameters were employed, except for torsion constants of rotation about the C.ar−N.pl3 and C.ar−C.2 bond types. These were increased to 12.0 kcal/mol to hinder unrealistic free rotation of the catechol−nitro and catechol−carbonyl bonds. For the genetic algorithm used in the conformation space exploration, a population of 100 individuals (conformations) was subjected to 105 mutational generations with a selection pressure of 1.1. All atoms at COMT molecular surface within a radius of 14.0 Å from the Mg^{2+} ion were used as the target binding site. The inhibitor's nitrocatechol moiety was docked with both hydroxyls protonated and Lys144 was considered unprotonated. The coordination of the catechol hydroxyl groups to Mg^{2+} is implicitly treated by GOLD as a special hydrogen bond, where the metal behaves as a hydrogen bond donor. Therefore, no constraints were used to force the catechol into the catalytic position. Finally, all docked structures (protein and inhibitor) were minimized with the molecular modeling package SYBYL (Tripos Inc., St. Louis, MO), using the MMFF94 force field.

Hydrophatic Interactions. Intermolecular hydrophatic interactions between COMT and the inhibitor (in either the crystallographic or docked configurations) were evaluated with the HINT algorithm,[31] as implemented in SYBYL version 6.9.1. Prior to HINT calculations, the Mg^{2+} ion and the catalytic water molecule HOH53 were deleted. Partitioning of the protein molecule was done using the dictionary method and inferring the ionization states of protein residues from their explicit hydrogen count. For the inhibitor, partitioning was calculated explicitly by applying corrective factors to polar proximity effects using the via-bond method. Polar interactions were directed along vectors coinciding with lone pairs or π orbitals. Stabilizing contributions to the HINT scores (negative values) include all acid−base, hydrophobic−hydrophobic interactions and hydrogen bonds, while counteracting contributions (positive scores) include acid−acid, base−base, and hydrophobic−polar interactions. Note that the sign notation used in this work is opposite to that of the original HINT scores.

Membrane Permeation. Prediction of blood−brain barrier permeation of **35** was performed with the VOLSURF algorithm,[32−34] as implemented in SYBYL version 6.9.1. The three-dimensional structure of **35** was generated from its connection table with CONCORD (Tripos Inc., St. Louis, MO) and the final structure optimized by energy minimization using MMFF94 force field. Three-dimensional interaction fields were first calculated around the target molecule, using the energy (Lennard-Jones, hydrogen bonding, and Coulombic electrostatics) of interaction with a molecular probe placed at each node of a regular 3D lattice. A grid resolution of 0.5 Å was employed, and three distinct molecular probes (water, DRY and carbonyl probes) were used to evaluate both polar and nonpolar molecular regions. In a subsequent step, VOLSURF transforms the rich information content of the 3D molecular fields into a set of scalar descriptors and projects their values onto a predictive model of blood−brain barrier permeation. The predictive model used in the present work was developed elsewhere,[23] by correlating the same set of descriptors with the experimental permeation of nearly 300 known drugs, using a cross-validated discriminant partial least squares procedure. Compound **35** was modeled in the neutral form, with catechol hydroxyls protonated and piperazine nitrogens unprotonated.

Supporting Information Available: Spectroscopic and microanalytical data for all synthesized compounds not included in the Experimental Section. This material is available free of charge via the Internet at http://pubs.acs.org.

References

(1) Axelrod, J.; Senoh, S.; Witkop, B. *O*-Methylation of catechol amines in vivo. *J. Biol. Chem*. **1958**, *233*, 697−701.
(2) Guldberg, H.; Marsden, C. Catechol−*O*-methyltransferase: Pharmacological aspects and physiological role. *Pharmacol. Rev*. **1975**, *27*, 135−206.
(3) Zhu, B. T.; Ezell, E. L.; Liehr, J. G. Catechol-*O*-methyltransferase-catalysed rapid *O*-methylation of mutagenic flavanoids. Metabolic inactivation as a possible reason for their lack of carcinogenicity in vitro. *J. Biol. Chem*. **1994**, *269*, 292−299.
(4) Burba, J. V.; Becking, G. C. Effect of the antioxidant norhydroguaiaretic acid on the in vitro activity of catechol-*O*-methyltransferase. *Arch. Int. Pharmacodyn. Ther*. **1969**, *180*, 323−329.
(5) Mannisto, P. T.; Kaakkola, S. New selective COMT inhibitors: Useful adjuncts for Parkinson's disease? *Trends Pharmacol. Sci*. **1989**, *10*, 54−56.
(6) Calne, D. B. Treatment of Parkinson's disease. *N. Engl. J. Med*. **1993**, *329*, 1021−1027.
(7) Messiha, F.; Hsu, T.; Bianchine, J. Peripheral aromatic L-amino acid decarboxylase inhibitor in parkinsonism. I. Effect on *O*-methylated metabolites of L-Dopa-2-^{14}C. *J. Clin. Invest*. **1972**, *51*, 452−455.
(8) Tohgi, H.; Abe, T.; Kikuchi, T.; Takahashi, S.; Nozaki, Y. The significance of 3-*O*-methyldopa concentrations in the cerebrospinal fluid in the pathogenesis of wearing-off phenomenon in Parkinson's disease. *Neurosci. Lett*. **1991**, *132*, 19−22.
(9) Borgulya, J.; Bruderer, H.; Bernauer, K.; Zurcher, G.; Da Prada, M. Catechol-O-methyltransferase-inhibiting pyrocatechol derivatives: Synthesis and structure−activity studies. *Helv. Chim. Acta*. **1989**, *72*, 952−968.
(10) Backstrom, R.; Honkanen, E.; Pippuri, A.; Kairisalo, P.; Pystynen, J.; Heinola, K.; Nissinen, E.; Lindén, I.-B.; Mannisto, P. T.; Kaakkola, S.; Pohto, P. Synthesis of some novel potent and selective catechol-*O*-methyltransferase inhibitors. *J. Med. Chem*. **1989**, *32*, 841−846.
(11) Borgulya, J.; Da Prada, M.; Dingemanse, J.; Scherschlicht, R.; Schlappi, B.; Zurcher, G. Ro 40−7592. Catechol-*O*-methyltransferase (COMT) inhibitor. *Drugs Future* **1991**, *16*, 719−721.
(12) Nissinen, E.; Lindén, I.-B.; Schultz, E.; Pohto, P. Biochemical and pharmacological properties of a peripherally acting catechol-*O*-methyltransferase inhibitor Entacapone. *Nauyn Schmiedebergs Arch. Pharmacol*. **1992**, *346*, 262−266.
(13) Assal, F.; Spahr, L.; Hadengue, A.; Rubbici-Brandt, L.; Burkhard, P. R. Tolcapone and fulminant hepaptitis. *Lancet* **1998**, *352*, 958.

(14) Learmonth, D. A.; Vieira-Coelho, M. A.; Benes, J.; Alves, P. C.; Borges, N.; Freitas, A. P.; Soares-da-Silva, P. Synthesis of 1-(3,4-dihydroxy-5-nitrophenyl)-2-phenylethanone and derivatives as potent and long-acting peripheral inhibitors of catechol-*O*-methyltransferase. *J. Med. Chem*. **2002**, *45*, 685−695.
(15) Almeida, L.; Soares-da-Silva, P. Pharmacokinetics and pharmacodynamics of BIA 3−202, a novel COMT inhibitor, during first administration to humans. *Drugs R&D* **2003**, *4*(4), 207−217.
(16) Almeida, L.; Soares-da-Silva, P. Pharmacokinetics and pharmacodynamic profiles of BIA 3-202, a novel catechol-*O*-methyltransferase (COMT) inhibitor, during multiple-dose administration to health subjects. *J. Clin. Pharmacol*. **2003**, *43*(12), 1350−1360.
(17) Costa, J. L.; Vieira-Coelho, M. A.; Soares-da-Silva, P. Catechol-*O*-methyltransferase activity in SK−N−SH cells. *Eur. J. Neurosci*. **2000**, *12*(suppl. 11), 280.
(18) Borges, N.; Vieira-Coelho, M. A.; Parada, A.; Soares-da-Silva, P. Studies on the tight-binding nature of tolcapone inhibition of soluble and membrane-bound rat brain catechol-*O*-methyltransferase. *J. Pharmacol. Exp. Ther*. **1997**, *282*, 812−817.
(19) Rodrigues, M. L.; Archer, M.; Bonifacio, M. J.; Soares-da-Silva, P.; Carrondo, M. A. Crystallization and preliminary crystallographic characterization of catechol-*O*-methyltransferase in complex with its cosubstrate and an inhibitor. *Acta Crystallogr.* **2001**, *D57*, 906−908.
(20) Bonifacio, M. J.; Archer, M.; Rodrigues, M. L.; Matias, P. M.; Learmonth, D. A.; Carrondo, M. A.; Soares-da-Silva, P. Kinetics and crystal structure of catechol-*O*-methyltransferase complex with co-substrate and a novel inhibitor with potential therapeutic application. *Mol. Pharmacol*. **2002**, *62*, 795−805.
(21) Cozzini, P.; Fornabaio, M.; Marabotti, A.; Abraham, D. J.; Kellogg, G. E.; Mozzarelli, A. Simple, intuitive calculations of free energy of binding for protein−ligand complexes. 1. Models without explicit constrained water. *J. Med. Chem.* **2002**, *45*, 2469−2483.
(22) Vidgren, J.; Svensson, L. A.; Liljas, A. Crystal structure of catechol-*O*-methyltransferase. *Nature* **1994**, *368*, 354−358.
(23) Crivori, P.; Cruciani, G.; Carrupt, P. A.; Testa, B. Predicting blood−brain barrier permeation from three-dimensional molecular structure. *J. Med. Chem.* **2000**, *43*, 2204−2216.
(24) Bernauer, K.; Borgulya, J.; Bruderer, H.; Da Prada, M.; Zurcher, G. US Patent No. 5,705,703, 1998.
(25) Guex, N.; Peitsch, M. C. SWISS-MODEL and the Swiss-PdbViewer: An environment for comparative protein modeling. *Electrophoresis* **1997**, *18*, 2714−2723.
(26) Zheng, Y. J.; Bruice, T. C. A theoretical examination of the factors controlling the catalytic efficiency of a transmethylation enzyme−Catechol-*O*-Methyltransferase. *J. Am. Chem. Soc.* **1997**, *119*, 8137−8145.
(27) Kuhn, B.; Kollman, P. A. QM-FE and molecular dynamics calculations on catechol-*O*-methyltransferase: Free energy of activation in the enzyme and in aqueous solution and regioselectivity of the enzyme-catalyzed reaction. *J. Am Chem. Soc.* **2000**, *122*, 2586−2596.
(28) Jones, G.; Willett, P.; Glen, R. C. A genetic algorithm for flexible molecular overlay and pharmacophore elucidation. *J. Comput.-Aided Mol. Des.* **1995**, *9*, 532−549.
(29) Jones, G.; Willett, P.; Glen, R. C. Molecular recognition of receptor sites using a genetic algorithm with a description of desolvation. *J. Mol. Biol.* **1995**, *245*, 43−53.
(30) Jones, G.; Willett, P.; Glen, R. C.; Leach, A. R.; Taylor, R. Development and validation of a genetic algorithm for flexible docking. *J. Mol. Biol.* **1997**, *267*, 727−748.
(31) Kellogg, G. E.; Joshi, G. S.; Abraham, D. J. New tools for modelling and understanding hydrophobicity and hydrophobic interactions. *Med. Chem. Rev.* **1992**, *1*, 444−453.
(32) Cruciani, G.; Pastor, M.; Clementi, S. Handling information from 3D grid maps for QSAR studies. *Molecular Modelling and Prediction of Bioactivity*; Kluwer Academic/Plenum Publishers: New York, 2000; pp 73−82.
(33) Cruciani, G.; Crivoni, P.; Carrupt, P.-A.; Testa, B. Molecular fields in quantitative structure−permeation relationships: The VolSurf approach. *J. Mol. Struct.* (*Theochem)* **2000**, *503*, 17−30.
(34) Cruciani, G.; Pastor, M.; Guba, W. VolSurf: A new tool for the pharmacokinetic optimization of lead compounds. *Eur. J. Pharm. Sci.* **2000**, *11*(Suppl 2), S29−39.

JM040848O